Protein glycosylation is essential for SARS-CoV-2 infection

Aitor Casas-Sanchez[1,2]*, Alessandra Romero-Ramirez[1,2§], Eleanor Hargreaves[3§], Edward I Patterson[1,2], Grant L Hughes[1,2], Tobias Zech[3], Álvaro Acosta-Serrano[1,2]

[1]Department of Vector Biology and [2]Department of Tropical Disease Biology, Liverpool School of Tropical Medicine, UK

[3]Department of Molecular and Cellular Physiology, University of Liverpool, UK

§ Equal contribution

*Corresponding author: aitor.casas-sanchez@lstmed.ac.uk

Keywords: SARS-CoV-2, COVID-19, coronavirus, *N*-glycosylation, *N*-glycan, viral infection.

Abstract

SARS-CoV-2 extensively *N*-glycosylates its surface spike (S) proteins. This post-translational modification is essential to modulate protein conformation and host cell invasion. Each S monomer can be modified with up to 22 *N*-glycans. To meet the high demand of protein glycosylation during virus replication, SARS-CoV-2 upregulates the expression of host *N*-glycosylation genes. Although a substantial amount of detail is known about the structure of S protein *N*-glycans, the role of *N*-glycosylation in SARS-CoV-2 infection remains largely undetermined. Here, we investigated the essentiality of the host *N*-glycosylation pathway and viral *N*-glycans for SARS-CoV-2 infection. When either monkey or human cells were preincubated with glycosylation inhibitors, including FDA-approved iminosugars, virus infection was significantly reduced. This infection phenotype was confirmed after RNAi knockdown of several glycosylation genes. In addition, enzymatic deglycosylation of whole viral particles confirmed that accessible oligosaccharides on the SARS-CoV-2 surface are essential for host cell infection. Altogether, we show evidence that the normal functioning of the host *N*-glycosylation machinery is essential not only for SARS-CoV-2 to infect, but also to produce new functional virions. These findings open the door for developing new approaches targeting *N*-glycosylation against COVID-19.

62 **Introduction**

63 The severe acute respiratory syndrome coronavirus 2 (SARS-CoV-2), responsible for
64 the COVID-19 pandemic, is a positive single-stranded RNA betacoronavirus
65 composed of four structural proteins that contain the viral genome[1]. The SARS-CoV-
66 2 surface spike glycoprotein has been extensively studied and is the target of most
67 vaccines and treatments under development due to its exposure, immunogenicity and
68 essential role in infection. It is well established that the main route for SARS-CoV-2 to
69 infect the host cell is via attachment to the receptor angiotensin-converting enzyme 2
70 (ACE-2) through the spike's receptor-binding domain (RBD), followed by membrane
71 fusion and invasion[2,3]. Both spike and ACE-2 are modified by the addition of a variable
72 number of *N*-glycans. While ACE-2 contains seven occupied glycosylation sites[4], the
73 homotrimeric spike protein has been shown to be heavily *N*-glycosylated with up to 66
74 oligosaccharides (22 per monomer) when recombinantly expressed in human HEK293
75 cells[5,6]. Cryo-electron microscopy has confirmed the presence of such glycans in real
76 SARS-CoV-2 virions[7]. Furthermore, it has been recently suggested that spike *N*-
77 glycans may play critical roles including proper protein folding and conformational
78 changes[8], successful recognition and attachment to ACE-2 and masking certain
79 epitopes to avoid antibody neutralization[3,5]. Most of these, however, are inferred from
80 computational models or resemblance to other viruses. There is little direct evidence
81 of the essentiality of spike *N*-glycans for SARS-CoV-2 infection. So far, only the use
82 of pseudotyped vesicular stomatitis virus (VSV) expressing the SARS-CoV-2 spike as
83 a proxy for the study of spike-driven host cell invasion has served useful for this
84 purpose[9]. By mutating *N*-glycosylation sites, it has been shown that the absence of
85 glycans on Asn^{331} and Asn^{343}, both within the RBD, resulted in a drastic reduction of
86 pseudovirus infection[10]. In addition, knocking out *MGAT1* gene, which encodes for *N*-
87 acetylglucosaminyl-transferase, an essential enzyme in the formation of hybrid and
88 complex *N*-glycans, also reduced invasion of pseudotyped VSV suggesting that hybrid
89 and complex spike *N*-glycans may be of importance for this process[11]. Although
90 SARS-CoV-2 cDNA clones have been available for months[12,13], no study has yet used
91 real virions to provide direct evidence.
92
93 The role of *N*-glycosylation, the main eukaryote protein post-translational modification,
94 in the context of a SARS-CoV-2 infection remains unknown to date. The *N*-
95 glycosylation pathway starts in the endoplasmic reticulum (ER) membrane where the

universal precursor $Glc_3Man_9GlcNAc_2$-dolichol-P is assembled in a stepwise manner. The glycan portion is then co-translationally added to an acceptor asparagine residue –within the sequon N-X-S/T; X≠P[14]– on a nascent polypeptide by STT3, the catalytic subunit of the oligosaccharyl-transferase (OST) complex[15]. The attached glycan is then modified by ER α-glucosidases I and II which remove the terminal glucose residues thus allowing the glycoprotein to enter into the calnexin/calreticulin quality control pathway and subsequent export to the Golgi apparatus[16]. In the Golgi, the oligomannosidic *N*-glycan gets trimmed by the action of several α-mannosidases and its structure can be further modified into a hybrid- or complex-type glycan thanks to the action of MGAT1[17]. The resulting glycan structure is highly variable depending on cell type and species. There are small molecules that can specifically inhibit enzymes along the *N*-glycosylation pathway, especially the α-glucosidase I. Although many of these compounds can be toxic, some are FDA-approved and used to treat human diseases such as type I Gauche disease (Miglustat[18]) or diabetes (Miglitol[19], Acarbose[20]). Others like Celgosivir, are in an advanced trial phase for their broad antiviral activity[21]. Previous drug screening studies have shown the efficacy of some of these and similar compounds against SARS-CoV-2[11,22-24].

In this study, we investigated the role of the host *N*-glycosylation pathway for SARS-CoV-2 infection *in vitro*. We found that by inhibiting key *N*-glycosylation steps using either chemical or genetic approaches, or by direct enzymatic deglycosylation, host cell infection is drastically inhibited. Thus, glycosylation of viral proteins represents a promising target against SARS-CoV-2 infection.

129 **Results**

130 <u>*N*-glycosylation inhibitors reduce SARS-CoV-2 infection *in vitro*</u>

131 We first hypothesized that the partial or complete inhibition of the host *N*-glycosylation
132 pathway may interfere with the normal development of a SARS-CoV-2 infection. This
133 drug-driven inhibition may either impede the normal processing and assembly of new
134 virions, hamper their capacity to infect further host cells and/or prevent the successful
135 recognition of cells presenting overall *N*-glycosylation defects, including key surface
136 receptors such as ACE-2. We tested 10 compounds known to inhibit key steps along
137 the *N*-glycosylation pathway, at concentrations considered to be at a low or high end
138 of the effective range. As inhibitors of the early pathway in the ER, we used
139 tunicamycin that prevents the formation of the *N*-glycan precursor, and NGI-1 that
140 inhibits the ER's oligosaccharyltransferase catalytic subunit STT3. Further in the
141 pathway, we inhibited ER α-glucosidase I using the iminosugars Miglitol, N-butyl-
142 deoxynojirimycin (Miglustat), 1-deoxynojirimycin (DNJ), N-Nonyldeoxynojirimycin
143 (NN-DNJ), Acarbose, Swainsonine and Celgosivir. In addition, we tested the efficacy
144 of Deoxymannojirimycin (DMM) as an inhibitor of Golgi α-mannosidase I. Pre-
145 incubation of either Vero E6 green monkey kidney epithelial cells or HEK293^{ACE-2}
146 (lentiviral overexpression of human ACE-2) human kidney cells with most inhibitors
147 prior to SARS-CoV-2 challenge (1 to 16 hours before infection), resulted in a significant
148 reduction in infection compared to untreated cells (**Figure 1**). The same protective
149 effect was observed when the inhibitors were added alongside the virus and up to 6
150 hours after infection (not shown). We determined the relative proportion of infection by
151 scanning whole wells and measuring the area occupied by infected (α-spike-positive)
152 cells in relation to the total (nuclei DAPI-stained) (**Figure 1a-c**). For selected inhibitors,
153 we measured the proportion of cells showing cytopathic effects (CPE) as a result of
154 the infection using crystal violet staining (**Figure 1d**) and quantified virus titres in cell
155 supernatants by plaque assay (**Figure 1e**). While untreated controls displayed most
156 cells as infected in clusters, both early inhibitors of the *N*-glycosylation pathway (i.e.,
157 tunicamycin and NGI-1) provided the highest protection rates against the virus in Vero
158 (97.3% and 97%) and HEK cells (92.3% and 92%), showing only few isolated infected
159 cells (**Figure 1a,b**). Tunicamycin and NGI-1 also protected cells against CPE (94%
160 and 99.5%) (**Figure 1d**) and at high doses led to undetectable levels of infectious
161 particles in cell supernatants, in a dose-dependent manner (**Figure 1e**). Inhibitors of

162 α-glucosidase I proved to be less effective and presented a greater variability. The
163 most effective ones (i.e., Miglustat, NN-DNJ and Celgosivir) showed reduced overall
164 infections in Vero and HEK cells, smaller clusters of infected cells, CPE protection and
165 moderate virus titre reduction in cell supernatants (**Figure 1**). Inhibition of the Golgi's
166 α-mannosidase I using DMM had no effect at preventing infection in Vero cells and a
167 slightly reduced infection in HEK cells. Viability assays using AlamarBlue were run in
168 parallel for all inhibitors to rule out poor metabolism or toxicity as the main causes for
169 infection decrease (**Figure 1e**).
170
171
172

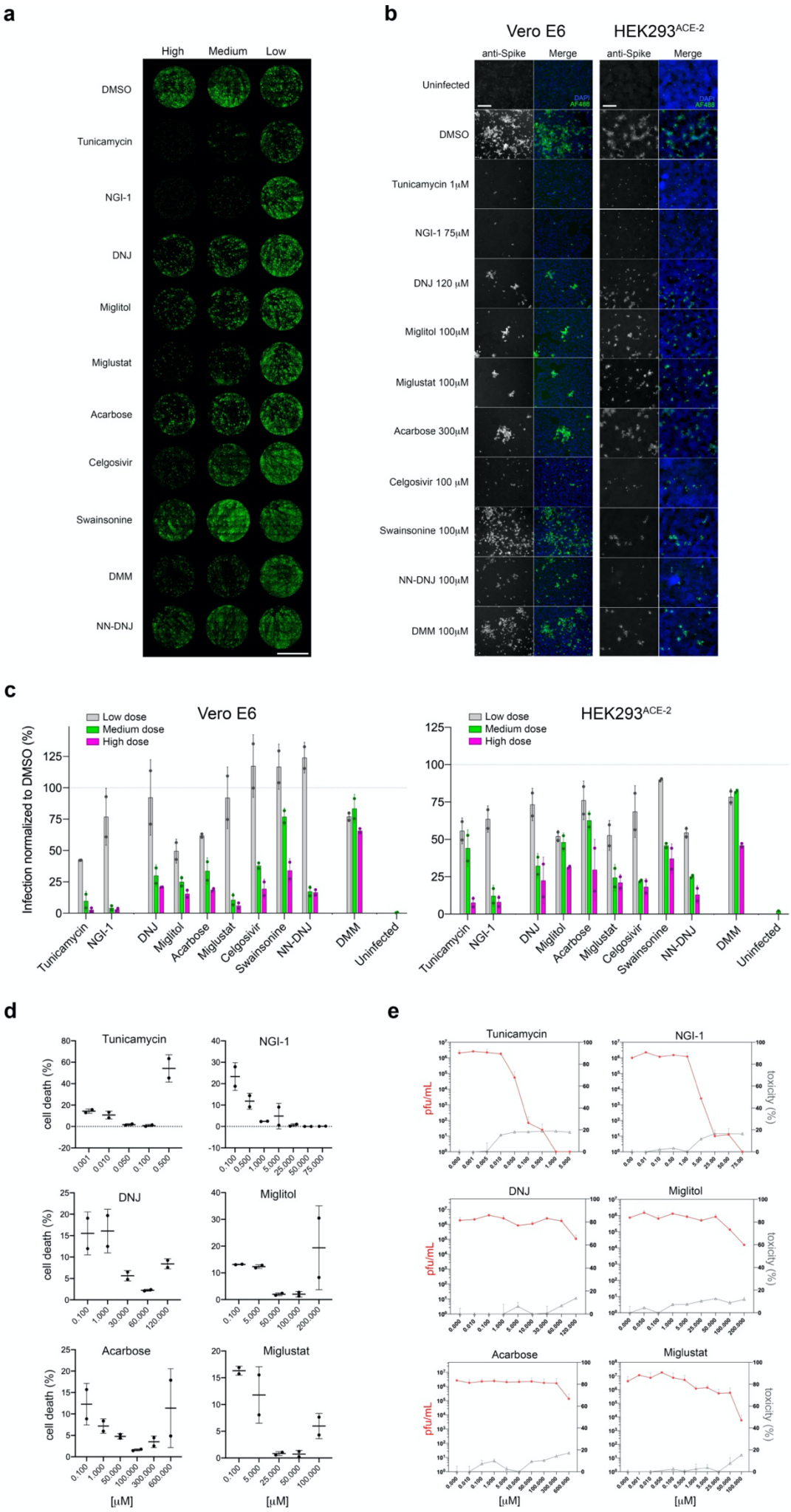
a
High
Medium
Low
DMSO
Tunicamycin
NGI-1
DNJ
Miglitol
Miglustat
Acarbose
Celgosivir
Swainsonine
DMM
NN-DNJ
b
Vero E6
HEK293ACE-2
anti-Spike
Merge
Uninfected
DMSO
Tunicamycin 1μM
NGI-1 75μM
DNJ 120 μM
Miglitol 100μM
Miglustat 100μM
Acarbose 300μM
Celgosivir 100 μM
Swainsonine 100μM
NN-DNJ 100μM
DMM 100μM
c
Vero E6
HEK293ACE-2
Low dose
Medium dose
High dose
Infection normalized to DMSO (%)
Tunicamycin
NGI-1
DNJ
Miglitol
Acarbose
Miglustat
Celgosivir
Swainsonine
NN-DNJ
DMM
Uninfected
d
Tunicamycin
NGI-1
DNJ
Miglitol
Acarbose
Miglustat
cell death (%)
[μM]
e
pfu/mL
toxicity (%)
[μM]

174 **Figure 1. Chemical inhibition of the host *N*-glycosylation pathway reduces SARS-CoV-2**
175 **infection *in vitro*.** (**a**) Representative whole-well scans of confluent Vero E6 monolayers treated
176 with either high, medium or low dose (see below) of several *N*-glycosylation inhibitors and infected
177 with SARS-CoV-2 (MOI=0.05, 24 hours). Cells immuno-stained using anti-spike antibodies
178 (green); DMSO untreated control; scale bar 5 mm. (**b**) Representative images of either Vero E6 or
179 HEK293^{ACE-2} cells in 'a' pre-treated with a high dose of *N*-glycosylation inhibitor and infected with
180 SARS-CoV-2 (MOI=0.05, 24 hours for Vero; MOI=0.1 for 24 hours for HEK293). Cells stained with
181 anti-Spike (grey channel) and merged (green) with DNA counterstain DAPI (blue); uninfected and
182 DMSO untreated controls included scale bars 200μm. (**c**) Quantification of the percentage of
183 infected (spike-positive) cells in 'a' normalized to DMSO controls (dashed horizontal line) of either
184 Vero E6 or HEK293^{ACE-2} cells pre-treated with inhibitors (at low, medium and high doses) and
185 infected with SARS-CoV-2 (MOI=0.05, 24 hours). Bars indicate the mean values; dots indicate
186 individual values; error bars represent standard deviation; two technical replicates; two
187 independent experiments performed. Inhibitor concentrations low, medium to high (μM):
188 tunicamycin (0.001, 0.01, 0.05); NGI-1 (0.001, 5, 75); DNJ (0.01, 60, 120); Miglitol (0.01, 50, 200);
189 Acarbose (0.01, 100, 300); Miglustat (0.01, 50, 100); Celgosivir, Swainsonine, NN-DNJ and DMM
190 (0.01, 25, 100). (**d**) Percentage of dead Vero E6 cells (area ratio of unstained cells with crystal
191 violet) pre-treated with glycosylation inhibitors after SARS-CoV-2 infection (MOI=0.001, 48 hours).
192 Line represents mean values, dots indicate individual values, error bars indicate standard
193 deviation; two technical replicates, two independent experiments performed. (**e**) Concentration of
194 infective viral particles (pfu/ml; in red) in supernatants of Vero E6 cells pre-treated with several
195 inhibitors and infected with SARS-CoV-2 (MOI=0.001 for 48 hours), determined by plaque assay
196 in Vero E6 cells. Toxicity percentage measured by AlamarBlue assay plotted alongside in grey.
197 Dots indicate the mean values; error bars represent standard deviation; two technical replicates
198 from two independent experiments.
199
200
201
202
203
204
205
206
207
208
209
210

211 Genetic ablation of the *N*-glycosylation pathway reduces SARS-CoV-2 infection
212 To validate the drug inhibition results, we used siRNAs to knock down genes encoding
213 for key enzymes in the *N*-glycosylation pathway prior to infection with SARS-CoV-2
214 (**Figure 2**). We knocked down 1) the OST's catalytic subunit STT3 (isoforms A, B and
215 both) to abolish transfer of *N*-glycan precursors to proteins, directly resembling the
216 inhibitory effects of NGI-1 and indirectly those of tunicamycin; 2) the GANAB catalytic
217 subunit of the ER α-glucosidase I to prevent the deglucosylation of *N*-glycans already
218 attached to proteins (emulating the effect that the α-glucosidase I inhibitors should
219 produce); and 3) the Golgi's MGAT1 enzyme to stop the formation of hybrid and
220 complex *N*-glycans. As expected, full knockdown of *STT3* (si*STT3A+B*) led to an
221 average infection reduction of ~55.4% in Vero and ~54.2% in HEK cells (**Figure 2a-**
222 **c**). To dissect out the contribution of each STT3 isoform, individual knockdowns were
223 also performed separately. While si*STT3-A* showed a profound inhibitory effect in HEK
224 cells (52% reduction), it did not result in significant virus reduction in Vero. On the
225 contrary, si*STT3-B* reduced the infection in Vero down to 48% but did not protect HEK
226 cells from infection. Reduction of *GANAB* levels further down in the pathway,
227 consistently resulted in less infections in both Vero and HEK cells, although the effect
228 was not as pronounced as seen in si*STT3* (41.4% and 42.5% respectively). Lastly,
229 si*MGAT1* had no effect in Vero but provided some protection to HEK cells (58.8%
230 infection). Knockdown levels were determined for each group and biological replicate
231 by immunoblotting using specific antibodies (**Figure 2d**).
232

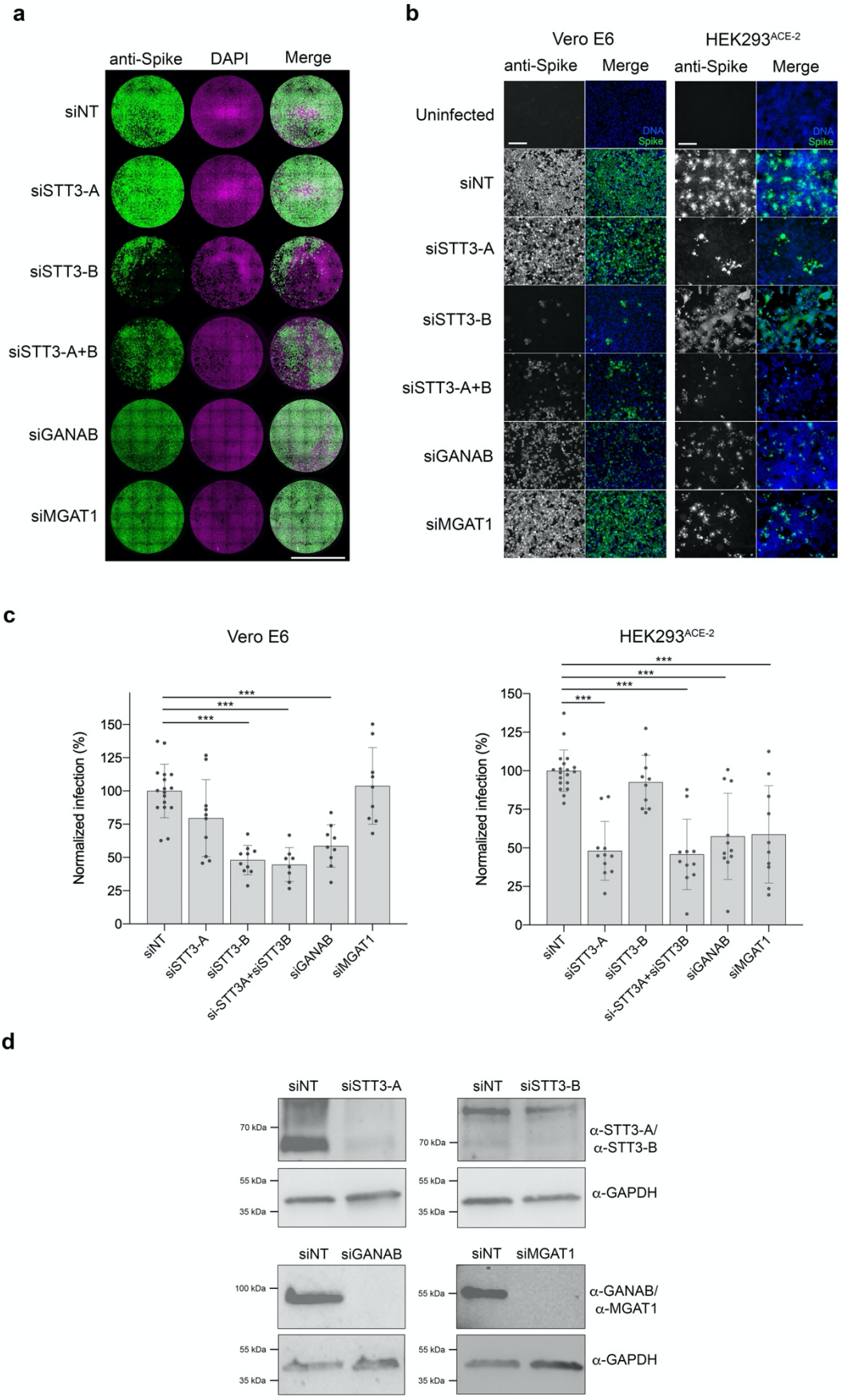

233
234
235
236

237 **Figure 2. Genetic ablation of host *N*-glycosylation genes reduces SARS-CoV-2 infectivity.**
238 (**a**) Representative whole-well scans of confluent Vero E6 monolayers transfected either with siNT
239 (negative control) or siRNAs for the knockdown of the *N*-glycosylation genes siSTT3-A, siSTT3-B,
240 siSTT3A+B, siGANAB and siMGAT1, and infected with SARS-CoV-2 (MOI=0.05, 24 hours). Cells
241 immunostained with anti-spike antibodies (green), counterstained with DAPI (purple) and merged;
242 scale bar 5 mm. (**b**) Representative images of either Vero E6 or HEK293^{ACE-2} siRNA cells infected
243 with SARS-CoV-2 (MOI=0.05 for 24 hours for Vero; MOI=0.1 for 24 hours for HEK293). Cells
244 immune-stained with anti-spike (gray channel) and merged (green) with DAPI counterstain (blue);
245 scale bars 200 μm. (**c**) Quantification of the percentage of infected (spike-positive) cells in 'a'
246 normalized to siNT controls of either Vero E6 or HEK293^{ACE-2} cells infected with SARS-CoV-2
247 (MOI=0.05, 24 hours for Vero; MOI=0.1 for 24 hours for HEK293). Bars indicate the mean values;
248 dots indicate individual values, error bars represent standard deviation; asterisks indicate
249 significance (p<0.001); three technical replicates, four independent experiments performed. (**d**)
250 Western blotting of protein lysates from Vero cells comparing siNT control cells with either
251 siSTT3-A, siSTT3-B, siGANAB or siMGAT1 cells probing with specific antibodies against the
252 knocked down protein, and with anti-GAPDH as loading control; apparent molecular weight
253 markers annotated on the left.
254
255
256
257 <u>SARS-CoV-2 *N*-glycans are essential for infection</u>
258 Having shown that the normal functioning of the host *N*-glycosylation machinery is
259 important for SARS-CoV-2 infection, we next wanted to determine whether viral *N*-
260 glycans alone also played a critical role. We hypothesized that glycoproteins in virions
261 assembled in cells with inhibited *N*-glycosylation may acquire abnormal *N*-
262 glycosylation profiles and consequently become less infectious. To test this
263 hypothesis, we used as model virions produced by Vero E6 cells treated with 5 μM
264 NGI-1. This treatment was previously observed to greatly reduce the proportion of
265 infected cells while allowing the formation of fewer infective viral particles. As
266 determined by plaque assay, supernatants from 5 μM NGI-1-treated cells contained
267 on average 392-fold less infective viral particles than untreated control cells (**Figure**
268 **3a**). However, quantification by qRT-PCR of total viral RNA (i.e., infective and non-
269 infective particles) in those same supernatants showed only a reduction of 82-fold in
270 NGI-1-treated cells compared to the control (**Figure 3b**). This difference between total
271 and infective particles (4.8-fold) may account for virions incapable of infecting host

272 cells as a result of altered and/or missing protein *N*-glycans. To validate this
273 hypothesis, the same supernatants were used to infect either untreated or 5 μM NGI-
274 1-treated Vero cells, normalizing the virus inoculum using RT-qPCR quantification
275 data. Despite having provided cells with virtually an identical amount of viral RNA, cells
276 infected with virions produced by NGI-1-treated cells still presented 4.4-fold less
277 infection, evidencing once more the existence of a sub-population of virions unable to
278 infect subsequent host cells (**Figure 3c**). As expected, NGI-1 treatment protected from
279 infection and made it even more pronounced when treated cells were infected with
280 NGI-1-derived virions. To confirm that the absence of *N*-glycans in certain viral
281 proteins renders viral particles non-infective, we performed *N*-glycan enzymatic
282 release on intact SARS-CoV-2 control virions prior to infection. Virions were purified
283 from cell supernatants by size exclusion and incubated with Peptide-N-Glycosidase F
284 (PNGase-F), which removes all types of *N*-linked oligosaccharides from glycoproteins.
285 Under this condition, the enzyme is only expected to cleave accessible *N*-glycans from
286 surface exposed viral glycoproteins (i.e., spike protein). Protein deglycosylation in
287 PNGase-F-treated virus lysate was confirmed by lectin blotting probing with either
288 concanavalin A (ConA) or wheat germ agglutinin (WGA) (**Figure 3d**), with overall lane
289 fluorescence intensity reductions of 57% and 70% respectively (**Figure 3e**). Some
290 visible protein bands (e.g., 120 kDa) also experienced a down shift in apparent
291 molecular weight due to the loss of *N*-glycans. After inoculation, Vero cells incubated
292 with PNGase-F-treated purified virions (PNGase-F +) remained uninfected, while cells
293 inoculated with purified virions incubated in the absence of the enzyme (PNGase-F -)
294 reached normal infection levels (~22%) comparable to those in cells inoculated with
295 purified virus only (29% infection) (**Figure 3f,g**). Control non-purified virions produced
296 a slightly higher average infection rate of 42%, proving that both steps of purification
297 and incubation with PNGase-F's reaction buffer had little impact on virion infectivity.
298 Supernatants of infected cells were collected to measure the amount of newly released
299 virions. Both total viral RNA quantification (**Figure 3h**) and plaque formation (**Figure**
300 **3i**) confirmed that cells infected with PNGase-F-treated virions did not develop a
301 SARS-CoV-2 infection.
302
303
304

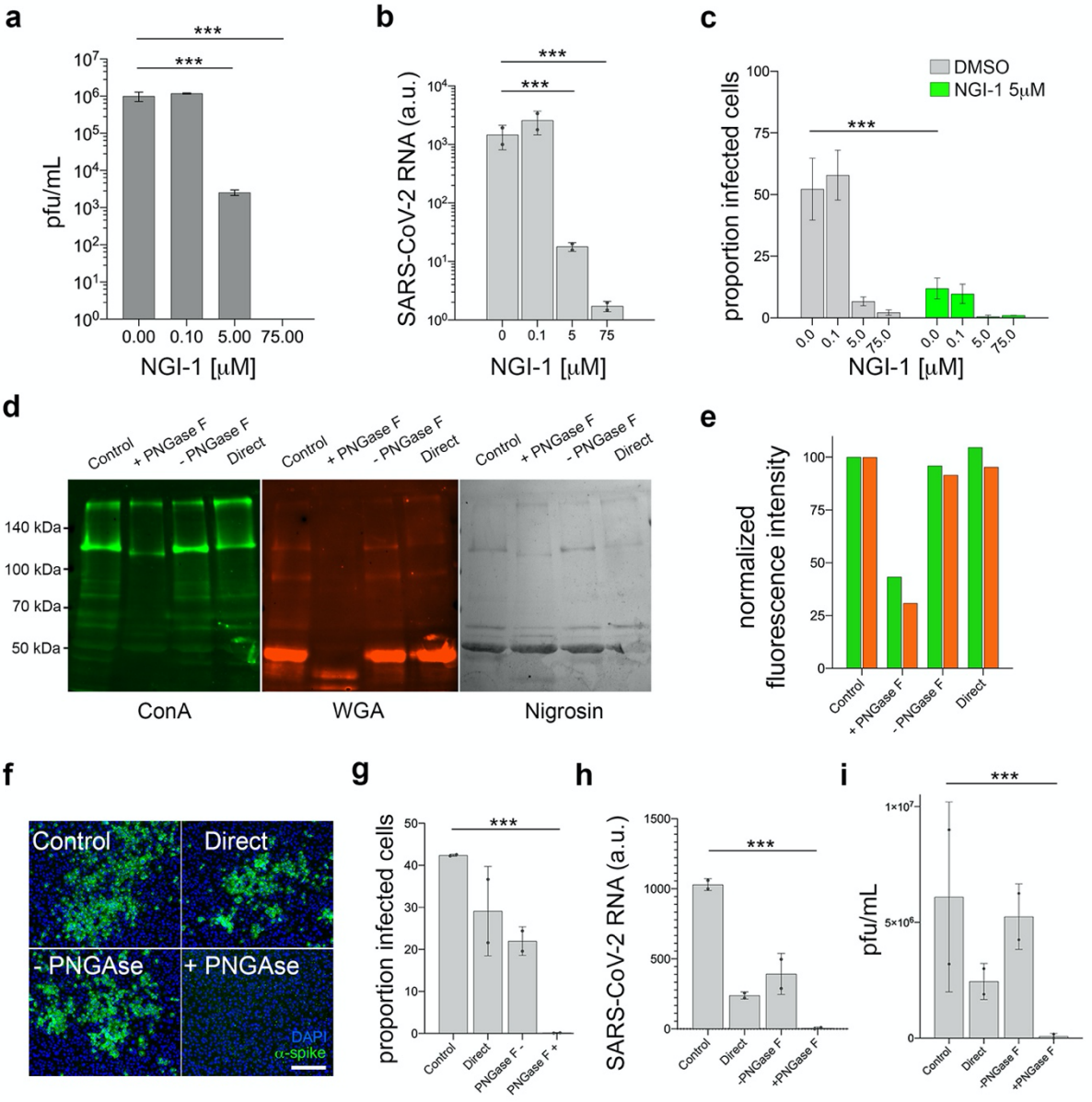

Figure 3. Surface exposed viral *N*-glycans are essential for infection. (**a**) SARS-CoV-2 titres (pfu/mL) measured by plaque assay in supernatants of Vero E6 infected cells (MOI=0.001, 48 hours) either treated with 0.1, 5, 75 μM NGI-1 or untreated (0); asterisks indicate significance (p<0.001). (**b**) Total SARS-CoV-2 RNA (arbitrary units) detected in supernatants in 'a' by RT-qPCR. (**c**) Proportion of Vero E6 spike-positive cells either treated with 0, 0.1, 5 or 75 μM NGI-1 infected with virus either from untreated (DMSO) or 5 μM NGI-1-treated cell supernatant, at MOI=0.05 for 24 hours normalized using total viral RNA data. (**d**) Lectin blotting of SARS-CoV-2-infected Vero E6 supernatant (Control), purified and PNGase F-treated for 5 hours at 37°C (+PNGase F), purified untreated (- PNGase F) or purified only (Direct) lysates. Membrane probed with ConA-FITC (green), WGA-rhodamine (red) and nigrosine-stained (white) afterwards for loading control. (**e**) Fluorescence intensity quantification of entire lanes in 'd' normalized to controls. (**f**) Representative images of Vero E6 cells infected with supernatants in 'd' (MOI=0.05, 24 hours), immuno-stained with anti-spike antibodies (green) and DAPI counterstain (blue); scale bar 200μm. (**g**) Quantification of the proportion of infected cells in 'f'. (**h**) Total SARS-CoV-2 RNA in supernatants produced in 'f' quantified by RT-qPCR. (**i**) SARS-CoV-2 titres measured in supernatants produced in 'f' by plaque assay.

320 **Discussion**

321 *N*-glycosylation, the main eukaryote protein post-translational modification, plays an
322 essential role in cell physiology. *N*-glycans can modulate protein folding, stability,
323 antigenicity and intermolecular interactions. Many human pathogenic viruses,
324 including SARS-CoV-2, *N*-glycosylate proteins involved in fundamental processes[25,6].
325 SARS-CoV-2 surface homotrimeric spike proteins, essential for cell host recognition
326 and invasion, are decorated with up to 22 *N*-glycans per monomer. It also *N*-
327 glycosylates the highly abundant nucleocapsid phosphoprotein (N) that envelops the
328 viral genetic material[26]. Although there is little evidence of *N*-glycosylation occurring in
329 other SARS-CoV-2 proteins, most are likely to be modified with *N*-glycans since many
330 contain canonical *N*-glycosylation sequons with enough predicted potential. Previous
331 studies have predicted that spike *N*-glycans may modulate protein folding and
332 multimerization[8], conformational changes, binding to the ACE-2 human receptor and
333 immunological shielding[5]. Also, it has been shown using recombinant proteins and
334 pseudotyped viruses that mutations in certain *N*-glycosylation sites of the spike lead
335 to reduced infectivity[10], and that treatment with kifunensine or MGAT1 knockout to
336 prevent the formation of complex *N*-glycans reduces pseudovirus infection[11].
337 However, the effects of altering *N*-glycosylation in SARS-CoV-2 virions remain
338 undetermined.

339

340 Here we investigated for the first time the essentiality of the host *N*-glycosylation
341 pathway and SARS-CoV-2 protein *N*-glycosylation in relation to infection, and whether
342 these could be potentially exploited to treat COVID-19. We hypothesized that
343 interfering with the host *N*-glycosylation pathway may negatively impact the SARS-
344 CoV-2 infection outcome because 1) newly synthesized viral proteins not properly *N*-
345 glycosylated could misfold or be non-functional; 2) newly assembled virions with *N*-
346 glycosylation defects could become non-infective; 3) host cell receptors (e.g., ACE-2)
347 presenting *N*-glycosylation defects could impede successful viral invasion of cells. We
348 found that the inhibition of key steps within the host *N*-glycosylation pathway using
349 known inhibitors greatly reduced SARS-CoV-2 infection and replication *in vitro,* in both
350 green monkey Vero E6 and human HEK293 kidney epithelial cells. Most inhibitors
351 reduced the overall number of infected cells, the number of cells presenting cytopathic
352 effect, and the viral load produced by these cells. We validated these results by
353 knocking down the expression of genes encoding for key enzymes in the *N*-

354 glycosylation pathway, including some the inhibitor targets (i.e., STT3 and GANAB).
355 The most effective infection inhibition was achieved when altering the early *N*-
356 glycosylation pathway, by either directly preventing the addition of the *N*-glycan
357 precursor $Glc_3Man_9GlcNAc_2$ to the nascent polypeptide (with NGI-1[27] and STT3
358 RNAi), or indirectly by blocking the formation of GlcNAc-dolichol phosphate using
359 tunicamycin. Interestingly, *STT3* isoform-specific knock down resulted in opposed
360 phenotypes in Vero and HEK cells. The knock down of *STT3-A*, responsible for the
361 co-translational glycosylation of most acceptor sites, only reduced viral infection in
362 human HEK cells but showed no impact in Vero cells despite an effective knock down
363 being achieved. STT3-B however, the isoform glycosylating those sites omitted by
364 STT3-A or close to the polypeptide ends in a post-translational manner, showed the
365 most pronounced effect in Vero cells that we could not replicate in HEK cells, likely
366 due to inefficient knock down. A similar phenotype for siSTT3-B was reported in Lassa
367 virus-infected cells[28]. Double knock down of *STT3-A* and *STT3-B* always resulted in
368 protection rates against infection similar to the effect caused by the most effective
369 isoform-specific knock down in cell type respectively. Moreover, we found that the
370 further downstream the *N*-glycosylation pathway is halted, the lesser the impact on
371 virus infectivity. Inhibition of the ER α-glucoside I, which removes the terminal α-
372 glucose residue from protein *N*-glycans, using either inhibitors or knock down of its
373 catalytic subunit GANAB, also resulted in reduced infectivity although not as high as
374 in early pathway inhibition. Not all α-glucosidase I inhibitors tested here were found to
375 be equally effective. While treatment with the iminosugars Miglustat, Celgosivir and
376 NN-DNJ led to a strong reduction of infection, CPE and viral load, others such as
377 Miglitol, DNJ, Acarbose or Swainsonine barely reduced the overall infection while
378 slightly protecting cells against CPE. Lastly, alterations later in the pathway either
379 using DMM to inhibit the Golgi's α-mannosidase I, or knocking down MGAT1 to
380 prevent the formation of hybrid and complex glycan types, resulted in no significant
381 infectivity decrease in Vero cells, and in a mild infection reduction in HEK cells.
382 Variations in the *N*-glycosylation profiles of both host cell and generated virions may
383 account for these differences observed between cell types.
384
385 The most potent inhibitors here used greatly reduced the overall number of infected
386 cells regardless the treatment timing, hours before, during or after infection. Unlike

387 untreated samples which displayed most infected cells in clusters, probably formed by
388 the spread of the virus from an infected cell to neighbouring ones, inhibitor-treated
389 samples showed discrete individual infected cells instead. These did also present
390 higher amounts of trapped spike protein, suggesting viral replication occurs but virions
391 cannot either assemble or egress properly for neighbour cells to become infected.
392 Experiments involving variable MOIs supported this hypothesis as the number of
393 infected cells in inhibitor-treated samples was proportional to the initial viral inoculum,
394 while untreated cells rapidly became fully infected. In addition, we hypothesized that
395 cells with inhibited *N*-glycosylation may be producing virions with glycosylation defects
396 that render them non-infective to further cells. We validated this hypothesis by
397 analyzing the supernatant of infected cells treated with a sub-inhibitory dose of NGI-1
398 and comparing the number of infective virions with the total amount of viral genetic
399 material. We found that indeed, these inhibitor-treated cells were producing a
400 significant population of virions uncapable of infecting further host cells, unlike
401 untreated cells which produced infective virions only. Further validation involved
402 enzymatic deglycosylation of intact virions, which rendered completely non-infective
403 viruses, evidencing the essential role of, at least, surface SARS-CoV-2 *N*-glycans for
404 infection.
405
406 It is expected that the blockage of the host *N*-glycosylation pathway and the
407 consequent removal or alteration of virus *N*-glycan structures have such a profound
408 impact in virus infectivity. Our results confirmed the predicted important roles of *N*-
409 glycans in relation to viral glycoprotein maturation, virion assembly and host cell
410 recognition and invasion. In addition, it likely has a remarkable impact because SARS-
411 CoV-2 has been shown to require upregulating genes along the *N*-glycosylation
412 pathway[29], especially those related with OST and glucosidase activities, likely to
413 ensure enough *N*-glycosylation capacity for the increased viral glycoprotein
414 production. The evidence generated in this study opens the door to further research
415 on developing ways to exploit the *N*-glycosylation inhibition and SARS-CoV-2 *N*-
416 glycans to treat COVID-19. Some of the inhibitors used here (i.e., Miglustat, Miglitol
417 and Acarbose) are FDA-approved drugs widely used to treat different unrelated
418 human diseases and could be considered for repurposing if found effective in trials,
419 alone or in combination. Celgosivir is in an advanced trial phase and could also be
420 considered. Also, drug discovery approaches may focus on identifying better and safer

421 OST inhibitors, especially against STT3-B, as a way to target viral *N*-glycosylation
422 more specifically. On the other hand, we have demonstrated that SARS-CoV-2
423 surface *N*-glycans are essential for infection. New potential treatments may consist of
424 blocking such glycans using antibodies or lectins to reduce and neutralize the spread
425 of the infection[30]. Concerns are currently arising about new SARS-CoV-2 variants that
426 could potentially escape treatments under development or vaccine-derived antibody
427 neutralization. Approaches targeting essential *N*-glycans may offer an advantage over
428 protein-based ones as *N*-glycosylation is a more conserved, independent protein
429 modification less favourable to mutation. In summary, the study of *N*-glycosylation in
430 relation to viral diseases may offer new and exciting opportunities to fight, not only
431 SARS-CoV-2, but further virus infections.

432 **Methods**

433 Cell culture and SARS-CoV-2 infection

434 Vero E6 cells (C1008; green African monkey kidney cells) were obtained from Public
435 Health England and cultured in DMEM medium (Lonza) supplemented with 10% fetal
436 bovine serum (FBS) (Gibco) and 50 μg/mL gentamicin (Sigma) at 37°C and 5% CO_2.
437 HEK293^{ACE-2} cells (lentiviral expression of human angiotensin-converting enzyme 2,
438 source) were cultured in DMEM supplemented with 10% FBS, 1mM sodium pyruvate
439 (Gibco) and 2 μg/mL puromycin (Invivogen) at 37°C and 5% CO_2. Cells were regularly
440 passaged (passage 2 to 30) by trypsinization when >80% confluence was reached.
441 SARS-CoV-2 isolate SARS-CoV-2/human/Liverpool/REMRQ0001/2020, isolated
442 from naso-pharyngeal swab from a patient, was passaged four times in Vero E6
443 cells[31]. Experimental cells were infected by incubation with SARS-CoV-2 (passage 4
444 in Vero E6) containing 2 x 10^7 pfu/mL in DMEM 2% FBS for 30 minutes at 37°C and
445 5% CO_2 with variable MOIs (see below).

446

447 *N*-glycosylation inhibitor assays

448 Cells were pre-treated for 2 to 16 hours before infection with either DMSO or several
449 *N*-glycosylation inhibitors (from DMSO stock solutions, DMSO final concentration
450 never exceeding 2%) in DMEM 2% FBS. Inhibitors used: Tunicamycin (Sigma), NGI-
451 1 (Sigma), DNJ (Cambridge Bioscience), Miglitol (Stratech Scientific), Miglustat
452 (Cambridge Bioscience), Acarbose (Fisher Scientific), NN-DNJ (Cambridge
453 Bioscience), Celgosivir (Sigma), DMM (Tebu-Bio) and Swainsonine (Cambridge
454 Bioscience). Cells were then infected by incubation with SARS-CoV-2 P4 supernatant
455 with the corresponding inhibitor for 30 minutes at 37°C and 5% CO_2, at either
456 MOI=0.001 (Vero E6 for plaque assay), MOI=0.05 or MOI=0.1 (Vero E6 and
457 HEK293^{ACE-2} for immunofluorescence assay, respectively). Cells were washed and left
458 in DMEM 2% FBS and *N*-glycosylation inhibitor at 37°C and 5% CO_2 for 48 hours
459 (Vero E6 for plaque assay) or 24 hours (Vero E6 and HEK293^{ACE-2} for
460 immunofluorescence). For toxicity assay, cells in 96-well plates were treated with
461 variable concentrations of inhibitors in DMEM 2% FBS in triplicate and after 24 hours,
462 AlamarBlue 10X solution (Invitrogen) was added and incubated for 4 hours at 37°C
463 before measuring well fluorescence intensity at 590 nm using a FLUOstar Omega
464 plate reader (BMG Labtech)

465 siRNA knockdowns

466 A total of 2 x 10^5 Vero E6 or HEK293^{ACE-2} cells were seeded in 6-well plates 24 hours
467 before transfection with one of the following siRNAs pools (Qiagen SMARTpool):
468 siSTT3A (catalogue number GS3703), siSTT3B (GS201595), siGANAB (catalogue
469 number: GS23193) or siMGAT1 (GS84061). Double knockdown of STT3A and STT3B
470 was performed by transfecting both siSTT3A and siSTT3B pools. Non-targeting
471 control (siNT) was obtained from Dharmacon. 4µL of siRNA were combined with 6µL
472 Lipofectamine RNAiMax (Invitrogen) in 200µL Opti-MEM (Gibco) and incubated for 20
473 minutes at RT before being added dropwise to the cells. 4 hours after transfection,
474 cells were flushed out with fresh medium. For siGANAB and siMGAT1, 2 hits of siRNA
475 over a 120-hour incubation period were performed. For siSTT3A, siSTT3B and
476 siSTT3A+siSTT3B, 3 hits of siRNA over a 168-hour period were needed. The day
477 before optimum knockdown (96 hours for 2 hits, 144 hours for 3 hits), cells were
478 trypsinized and 2 x 10^4 cells for each condition were seeded onto 96-well optical plates
479 (Greiner) in quadruplicate and infected the following day. Infections were carried out
480 by incubation with SARS-CoV-2 P4 supernatant at either MOI=0.05 (Vero E6) or
481 MOI=0.1 (HEK293^{ACE-2}) for 30 minutes at 37°C, 5% CO_2, washing and incubation in
482 DMEM 2% FBS 37°C, 5% CO_2 for 24 hours.
483
484 Plaque assay
485 Vero E6 were cultured in DMEM 10% FBS in 24-well plates and allowed to reach
486 confluency overnight. Cells were incubated with 0.1 mL serially diluted supernatant
487 containing SARS-CoV-2 for 30 minutes at 37°C and 5% CO_2 before being discarded.
488 Cells were then washed in DMEM 2% FBS and left in 1.5mL overlay (DMEM 2%FBS,
489 1.2% Avicel) at 37°C and 5% CO_2 for 72 hours. Cells were fixed in formaldehyde for
490 30 minutes, washed in water and stained with 0.1% crystal violet solution (in 20%
491 ethanol) for manual plaque counting.
492
493 PNGase-F glycan enzymatic release
494 0.5mL SARS-CoV-2 P4 supernatant containing 2 x 10^7 pfu/mL was purified using an
495 Amicon Ultra (MWCO 100kDa) column (Merck) by centrifugation and washing in PBS
496 at 2,000xg. 18uL purified supernatant (containing 9x10^5 pfu) were combined with
497 recombinant glycerol-free PNGase-F and Glycobuffer 2 (New England Biolabs)
498 following the manufacturer's protocol for non-denaturing digestion, and incubated at

499 37°C for 5 hours. Parallel controls included incubation of purified virions without
500 PNGase-F and without both PNGase-F and buffer. After incubation, samples were
501 either directly used for infection or combined with RIPA buffer supplemented with
502 protease inhibitors for blotting.
503
504 RT-qPCR SARS-CoV-2 quantification
505 Total RNA was extracted from supernatants of SARS-CoV-2-infected Vero E6 cells
506 using the RNeasy kit (Qiagen) following the manufacturer's protocol. 4 μL purified RNA
507 were subsequently used for RT-qPCR reaction using the Luna Universal One-Step
508 RT-qPCR kit (New England Biolabs) and 0.4μM of each primer: CoV2-N-F
509 (CACATTGGCACCCGCAATC) and CoV2-N-R (GAGGAACGAGAAGAGGCTTGAC).
510 Reactions were set and analyzed in an Agilent Mx3005P machine as follows: 55°C for
511 10 minutes, 95°C for 1 minute, 40 cycles of 95°C for 10 seconds followed by 60°C for
512 30 seconds (SYBR green measure), with final melting curve from 55°C to 95°C.
513 Samples were quantified using the ΔCt method.
514
515 Immunofluorescence assay
516 Cells cultured in optical plates were fixed in 4% formaldehyde (Pierce) for 30 minutes,
517 washed in PBS and permeabilized in 0.5% saponin for 10 minutes. Cells were then
518 blocked in 1% bovine serum albumin (BSA) for 45 minutes and further incubated in
519 blocking solution containing anti-SARS-CoV-2 spike protein (S) subunit 1 (Abcam)
520 1:1000 dilution for 1 hour at 37°C. Blocking solution was then incubated for 1 hour at
521 RT containing DAPI 1μg/mL and anti-mouse IgG Alexa Fluor 488 Plus-conjugated
522 (Thermofisher). Cells were washed and left in PBS for imaging. Imaging was carried
523 out using a Zeiss LSM800 confocal laser scanning microscope by tile-scanning entire
524 wells or plates conserving identical settings between comparable samples. Images
525 were analyzed using Fiji (ImageJ) by thresholding to select positive signals only and
526 measuring area coverage of DAPI channel (total number of cells) and mean intensity
527 of the Alexa Fluor channel (infected cells).
528
529 Western blotting
530 Cell lysates were obtained at either 120-hours (2 hits) or 168-hours (3 hits). Cells were
531 washed in cold PBS 3 times and incubated in RIPA buffer with 1% phosphatase and

532 protease inhibitor cocktail (ThermoScientific) for 10 minutes on ice before scrapping,
533 centrifuging at 15,000 rpm for 10 minutes at 4°C and collecting the supernatants.
534 Protein concentration was determined using Precision Red (Cytoskeleton) and 60µg
535 of protein were separated using 4-15% SDS-PAGE gels (BioRad) and transferred onto
536 nitrocellulose membrane (GE) using a BioRad Trans-Blot Turbo Transfer system.
537 Membranes were blocked in either 5% milk or 2% BSA in Tris-buffered saline, 0.1%
538 Tween-20 (TBS-T) for 30 minutes at RT and incubated with their corresponding
539 primary antibodies at 4°C overnight. Primary antibodies used: anti-STT3A
540 (HPA030735, Cambridge Bioscience), anti-STT3B (A15574, Universal Biologicals),
541 anti-GANAB (A13851, Universal Biologicals), anti-MGAT1 (CSB-PA013773ESR1Hu,
542 2B Scientific) and anti-GAPDH (10494-1-AP, ProteinTech). Blots were then washed 3
543 times under agitation for 5 minutes in TBS-T before incubation with horseradish
544 peroxidase (HRP)-conjugated anti-rabbit IgG secondary antibody (Cell Signalling) for
545 1 hour at RT. After washing, blots were visualized on a ChemiDoc™ Touch Gel
546 Imaging System (BioRad) using enhanced chemiluminescence substrate (BioRad).
547 GAPDH was utilized as loading control for all blots.
548
549 Lectin blotting
550 Cell lysates of siRNA and *N*-glycosylation inhibitor-treated cells were obtained as
551 described above. 60µg protein was separated in 12.5% SDS-PAGE gels, transferred
552 onto nitrocellulose membranes and blocked in 1% BSA PBS overnight at 4°C. Blots
553 were incubated in 1% BSA containing both concanavalin A (ConA) FITC-conjugated
554 (1 µg/mL) and wheat germ agglutinin (WGA) rhodamine-conjugated (1µg/mL) (Vector
555 Labs) for 30 minutes at RT. After extensive washing in PBS 0.05% Tween-20,
556 membranes were imaged using a Thermofisher iBright FL1500 system.
557
558
559
560
561
562
563
564

Financial support

This work was supported in part by the Liverpool School of Tropical Medicine Director's Catalyst Fund awarded to ACS and the UKRI-BBSRC COVID rolling fund (BB/V017772/1) awarded to AAS, ACS, EIP and GLH. GLH was supported by the BBSRC (BB/T001240/1 and V011278/1), a Royal Society Wolfson Fellowship (RSWF\R1\180013), the NIH (R21AI138074), UKRI (20197), and the NIHR (NIHR2000907). GLH is affiliated to the National Institute for Health Research Health Protection Research Unit (NIHR HPRU) in Emerging and Zoonotic Infections at University of Liverpool in partnership with Public Health England (PHE), in collaboration with Liverpool School of Tropical Medicine and the University of Oxford. GLH is based at LSTM. The views expressed are those of the author(s) and not necessarily those of the NHS, the NIHR, the Department of Health or Public Health England. Confocal imaging facilities at LSTM were funded by a Wellcome Trust Multi-User Equipment Grant (104936/Z/14/Z).

Author Contributions

ACS and AAS conceptualized and designed the study. ACS, ARR, EH, TZ performed the experiments. ACS, ARR, EH, EIP, GLH, TZ, AAS analyzed, curated and validated data. ACS wrote the paper with input from all the authors.

Competing interests

The authors declare no competing interests.

599 **References**

600 1. Lu, R. *et al.* Genomic characterisation and epidemiology of 2019 novel
601 coronavirus: implications for virus origins and receptor binding. *Lancet* **395,**
602 565–574 (2020).
603 2. Hoffmann, M. *et al.* SARS-CoV-2 Cell Entry Depends on ACE2 and TMPRSS2
604 and Is Blocked by a Clinically Proven Protease Inhibitor. *Cell* **181,** 271–280.e8
605 (2020).
606 3. Walls, A. C. *et al.* Structure, Function, and Antigenicity of the SARS-CoV-2
607 Spike Glycoprotein. *Cell* (2020). doi:10.1016/j.cell.2020.02.058
608 4. Shajahan, A. *et al.* Comprehensive characterization of N- and O- glycosylation
609 of SARS-CoV-2 human receptor angiotensin converting enzyme 2.
610 *Glycobiology* (2020). doi:10.1093/glycob/cwaa101
611 5. Watanabe, Y., Allen, J. D., Wrapp, D., McLellan, J. S. & Crispin, M. Site-
612 specific glycan analysis of the SARS-CoV-2 spike. *Science* eabb9983 (2020).
613 6. Shajahan, A., Supekar, N. T., Gleinich, A. S. & Azadi, P. Deducing the N- and
614 O-glycosylation profile of the spike protein of novel coronavirus SARS-CoV-2.
615 *Glycobiology* **30,** 981–988 (2020).
616 7. Yao, H. *et al.* Molecular Architecture of the SARS-CoV-2 Virus. *Cell* (2020).
617 8. Casalino, L. *et al.* Beyond Shielding: The Roles of Glycans in the SARS-CoV-2
618 Spike Protein. *ACS Cent Sci* **6,** 1722–1734 (2020).
619 9. Dieterle, M. E. *et al.* A replication-competent vesicular stomatitis virus for
620 studies of SARS-CoV-2 spike-mediated cell entry and its inhibition. *Cell Host*
621 *Microbe* (2020). doi:10.1016/j.chom.2020.06.020
622 10. Li, Q. *et al.* The Impact of Mutations in SARS-CoV-2 Spike on Viral Infectivity
623 and Antigenicity. *Cell* (2020). doi:10.1016/j.cell.2020.07.012
624 11. Yang, Q. *et al.* Inhibition of SARS-CoV-2 viral entry upon blocking N- and O-
625 glycan elaboration. *Elife* **9,** 450 (2020).
626 12. Thao, T. T. N. *et al.* Rapid reconstruction of SARS-CoV-2 using a synthetic
627 genomics platform. *Nature* 1–27 (2020). doi:10.1038/s41586-020-2294-9
628 13. Xie, X. *et al.* An Infectious cDNA Clone of SARS-CoV-2. *Cell Host Microbe* **27,**
629 841–848.e3 (2020).
630 14. Gavel, Y. & Heijne, von, G. Sequence differences between glycosylated and
631 non-glycosylated Asn-X-Thr/Ser acceptor sites: implications for protein
632 engineering. *Protein Eng* **3,** 433–442 (1990).
633 15. Helenius, A. & Aebi, M. Roles of N-linked glycans in the endoplasmic
634 reticulum. *Annu Rev Biochem* **73,** 1019–1049 (2004).
635 16. Herscovics, A. Importance of glycosidases in mammalian glycoprotein
636 biosynthesis. *Biochim Biophys Acta* **1473,** 96–107 (1999).
637 17. Schachter, H. *The joys of HexNAc. The synthesis and function of N- and O-*
638 *glycan branches. Glycoconjugate journal* **17,** 465–483 (Kluwer Academic
639 Publishers-Plenum Publishers, 2000).
640 18. Cox, T. M. *et al.* The role of the iminosugar N-butyldeoxynojirimycin (miglustat)
641 in the management of type I (non-neuronopathic) Gaucher disease: a position
642 statement. *J Inherit Metab Dis* **26,** 513–526 (2003).
643 19. Scott, L. J. & Spencer, C. M. Miglitol: a review of its therapeutic potential in
644 type 2 diabetes mellitus. *Drugs* **59,** 521–549 (2000).
645 20. Campbell, L. K., White, J. R. & Campbell, R. K. Acarbose: its role in the
646 treatment of diabetes mellitus. *Ann Pharmacother* **30,** 1255–1262 (1996).
647 21. Durantel, D. Celgosivir, an alpha-glucosidase I inhibitor for the potential
648 treatment of HCV infection. *Curr Opin Investig Drugs* **10,** 860–870 (2009).

22. Marcello, A. *Repurposing of Miglustat to inhibit the coronavirus Severe Acquired Respiratory Syndrome SARS-CoV-2*. *bioRxiv* 1–17 (2020). doi:10.1101/2020.05.18.101691
23. Williams, S. J. & Goddard-Borger, E. D. α-glucosidase inhibitors as host-directed antiviral agents with potential for the treatment of COVID-19. *Biochem Soc Trans* (2020).
24. Clarke, E. C., Nofchissey, R. A., Ye, C. & Bradfute, S. B. The iminosugars celgosivir, castanospermine and UV-4 inhibit SARS-CoV-2 replication. *Glycobiology* (2020). doi:10.1093/glycob/cwaa091
25. Watanabe, Y. *et al.* Vulnerabilities in coronavirus glycan shields despite extensive glycosylation. *Nat Commun* **11,** 2688–10 (2020).
26. Supekar, N. T. *et al.* SARS-CoV-2 Nucleocapsid protein is decorated with multiple N- and O-glycans. *bioRxiv* 2020.08.26.269043 (2020).
27. Puschnik, A. S. *et al.* A Small-Molecule Oligosaccharyltransferase Inhibitor with Pan-flaviviral Activity. *Cell Rep* **21,** 3032–3039 (2017).
28. Zhu, S. *et al.* Comprehensive Interactome Analysis Reveals that STT3B Is Required for N-Glycosylation of Lassa Virus Glycoprotein. *J. Virol.* **93,** e01443–19 (2019).
29. Oommen, A., Cunningham, S. & Joshi, L. Transcriptomic Analysis of Respiratory Tissue and Cell Line Models to Examine Glycosylation Machinery during SARS-CoV-2 Infection. *Viruses* **13,** (2021).
30. da Silva, L. C. N. *et al.* Exploring lectin-glycan interactions to combat COVID-19: lessons acquired from other enveloped viruses. *Glycobiology* (2020). doi:10.1093/glycob/cwaa099
31. Patterson, E. I. *et al.* Methods of Inactivation of SARS-CoV-2 for Downstream Biological Assays. *J Infect Dis* **222,** 1462–1467 (2020).